LIMNOLOGY
and
OCEANOGRAPHY

ASLO

Limnol. Oceanogr. 62, 2017, 2260–2276
© 2017 Association for the Sciences of Limnology and Oceanography
doi: 10.1002/lno.10565

Light availability rather than Fe controls the magnitude of massive phytoplankton bloom in the Amundsen Sea polynyas, Antarctica

Jisoo Park,[1] Fedor I. Kuzminov,[2] Benjamin Bailleul,[2,a] Eun Jin Yang,[1] SangHoon Lee,[1] Paul G. Falkowski,[2] Maxim Y. Gorbunov [2]*

[1]Korea Polar Research Institute, Yeonsu-Gu, Incheon, South Korea
[2]Department of Marine and Coastal Sciences, Rutgers, The State University of New Jersey, New Brunswick, New Jersey

Abstract

Amundsen Sea polynyas are among the most productive, yet climate-sensitive ecosystems in the Southern Ocean and host massive annual phytoplankton blooms. These blooms are believed to be controlled by iron fluxes from melting ice and icebergs and by intrusion of nutrient-rich Circumpolar Deep Water, however the interplay between iron effects and other controls, such as light availability, has not yet been quantified. Here, we examine phytoplankton photophysiology in relation to Fe stress and physical forcing in two largest polynyas, Amundsen Sea Polynya (ASP) and Pine Island Polynya (PIP), using the combination of high-resolution variable fluorescence measurements, fluorescence lifetime analysis, photosynthetic rates, and Fe-enrichment incubations. These analyses revealed strong Fe stress in the ASP, whereas the PIP showed virtually no signatures of Fe limitation. In spite of enhanced iron availability in the PIP, chlorophyll biomass remained $\sim$ 30–50% lower than in the Fe-stressed ASP. This apparent paradox would not have been observed if iron were the main control of phytoplankton bloom in the Amundsen Sea. Long-term satellite-based climatology records revealed that the ASP is exposed to significantly higher solar irradiance levels throughout the summer season, as compared to the PIP region, suggesting that light availability controls the magnitude of phytoplankton blooms in the Amundsen Sea. Our data suggests that higher Fe availability (e.g., due to higher melting rates of ice sheets) would not necessarily increase primary productivity in this region. Furthermore, stronger wind-driven vertical mixing in expanding ice-free areas may lead to reduction in light availability and productivity in the future.

The Amundsen Sea is a climate-sensitive region where glaciers and ice cover have been declining most rapidly in the Antarctic over the past several decades (Walker et al. 2007; Rignot et al. 2008). This change is largely driven by the intrusion of relatively warm, salty, and nutrient-rich Circumpolar Deep Water (CDW), which accelerates melting of floating ice sheets in the Amundsen Sea (Walker et al. 2007; Vaughan 2008; Jenkins et al. 2010; Wåhlin et al. 2010; Jacobs et al. 2011), as well as by the ice thinning on the nearby Antarctic Continent (Rignot et al. 2008). Amundsen Sea Polynya (ASP) is one of the largest and most productive coastal polynyas in the Southern Ocean. The ASP is formed in the austral spring and summer, reaching it maximum open water area of $>60{,}000$ km^2 in February, though this area exhibits substantial interannual variations (Arrigo et al. 2012). Pine Island Polynya (PIP) is generally smaller and its size exhibits even greater interannual variability (Arrigo et al. 2012). Satellite-based ocean color data revealed that the Amundsen polynyas host massive annual phytoplankton blooms, which generally start about 1 month after the opening of the polynyas and peaks in mid-January when the polynyas are still expanding (Arrigo et al. 2012). The phytoplankton bloom in the ASP lasts about 2 weeks longer and reaches about 30% higher primary productivity per unit area than that in the PIP (Arrigo et al. 2012). However, it remains unclear why phytoplankton productivity and biomass in the ASP is higher than that in the PIP.

In the Southern Ocean, the most productive waters are confined to the continental shelves (Arrigo et al. 2008; Smith and Comiso 2008), downstream of islands (Korb et al. 2004), regions of pronounced topographic effects that promote local upwelling (Park et al. 2010), and polynyas (Arrigo and

[a]Present address: Institut de Biologie Physico-Chimique (IBPC), UMR 7141, Centre National de la Recherche Scientifique (CNRS), Université Pierre et Marie Curie, Paris, France

*Correspondence: gorbunov@marine.rutgers.edu

Van Dijken 2003; Lee et al. 2012). Satellite data revealed that, among the 37 identified polynyas in the Antarctic, ASP and PIP are among the most productive regions (per unit area) of the Southern Ocean (Arrigo and Van Dijken 2003). For instance, the ASP exhibits $\sim$ 50% larger air-sea CO_2 flux than the Ross Sea and most of continental shelves around the world (Mu et al. 2014). The physical and biogeochemical controls that support this unusually high productivity remain poorly understood due to the geographical isolation and a very limited amount of in situ data in this region.

In the Southern Ocean, concentrations of the macronutrients, nitrate, phosphate, and silicate, remain high throughout the year and primary productivity is limited by the paucity of iron and by light (De Baar et al. 1995; Sunda and Huntsman 1997). Phytoplankton cells require iron to maintain iron-rich components of the photosynthetic electron transport chain and reaction centers (Krause and Weis 1991; Falkowski et al. 1992). As cellular Fe requirements and uptake rates vary markedly between phytoplankton species (Sunda and Huntsman 1997; Alderkamp et al. 2012*a*), measurements of Fe concentrations alone are not sufficient to assess the effects of this micronutrient on phytoplankton growth and physiology. Variable fluorescence signals from phytoplankton photosystem II (PSII) are particularly sensitive to iron limitation (Greene et al. 1992; Vassiliev et al. 1995) and are readily used as an instantaneous indicator of the physiological status of phytoplankton in response to iron stress without conducting labor-intensive incubations (Falkowski et al. 2004).

In the polynyas, austral summer Fe supply usually remains high due to input from melting sea ice (Martin et al. 1990; Sedwick et al. 2000; El-Sayed 2005), glaciers (Alderkamp et al. 2012*b*; Gerringa et al. 2012), and floating icebergs (Smith et al. 2007). In spite of substantial influxes of iron from surrounding ice and icebergs, phytoplankton growth in polynyas may become Fe-limited in late austral summer, as has been observed in the Ross Sea Polynya (Sedwick et al. 2000; Tagliabue and Arrigo 2005). While it is possible that substantial Fe supply from melting glaciers could dynamically fuel a phytoplankton bloom in the ASP (Alderkamp et al. 2012*b*; Gerringa et al. 2012), biophysical signatures of Fe limitation have been observed here even at early stages of the bloom development (Alderkamp et al. 2015). Contemporary models of bloom dynamics in the Southern Ocean (Holm-Hansen and Mitchell 1991; Mitchell and Holm-Hansen 1991; Nelson and Smith 1991) suggest that the bloom development may be terminated when phytoplankton production rates become light limited due to strong self-shading by high standing stocks and when the mixed layer depth (MLD) approaches the critical depth (CRD), where net phytoplankton growth is compensated by integrated losses (Sverdrup 1953; Smetacek and Passow 1990). In contrast, it has been proposed that in the ASP, paucity of iron is the main limiting factor of the bloom development (Alderkamp et al. 2012*b*, 2015; Thuróczy et al. 2012).

Here, we consider and test two alternative hypotheses for the bottom-up controls and limiting factors of phytoplankton blooms in the Amundsen Sea. When the top-down effects, such as grazing pressure, remain invariant, these hypotheses predict two different patterns of bloom dynamics in relation to environmental forcing. If the paucity of iron is the main limiting factor of bloom dynamics (Hypothesis 1), then the water masses with similar physical conditions but higher Fe availability should exhibit higher phytoplankton biomass. In contrast, if light availability is the main limiting factor (Hypothesis 2), then higher biomass will be observed in areas exposed to higher irradiance levels.

In order to test these two alternative hypotheses, we analyzed spatial distributions of phytoplankton physiology and physical controls of phytoplankton growth in two of the largest Amundsen Sea polynyas with strikingly different signatures of Fe stress and productivity. This research was conducted at the late stage of bloom development from 10 February 2012 to 10 March 2012 aboard the icebreaker Araon as part of the Korea Antarctic Research Program (Fig. 1). Our assessment of the iron stress employs variable fluorescence measurements, picosecond fluorescence lifetime analysis, and Fe enrichment experiments in on-deck incubators. To quantify the importance of light limitation in controlling the bloom development, we employed the classical Sverdrup's concept of CRD (Sverdrup 1953) and analyzed variations in CRDs in relation to MLDs. We also measured photosynthetic rates as a function of photosynthetically available radiation (PAR) and depth and showed that these rates averaged over the mixed layer are almost an order of magnitude lower than their potential maximum, suggesting severe light limitation of photosynthesis. We further examined long-term satellite-based climatology records of physical forcing (wind speed and insolation) to better understand the importance of these controls in bloom dynamics. Our results provide the first in situ observations that reveal a Fe-driven difference in phytoplankton photophysiological status between the two Amundsen polynyas, however, the entire set of biogeochemical and biophysical data clearly suggest that light availability rather than Fe has more influence over the bloom development and dynamics in this climate-sensitive region.

Methods

Observations

A SeaBird SBE 911 CTD mounted on the Rosette system was operated at sea. Vertical profiles of temperature and salinity from the CTD were used to determine the MLD. The MLD was defined as the depth at which the water density increased abruptly. A PAR sensor on the CTD Rosette was used for logging underwater irradiances. The euphotic depth was defined as the depth at which the irradiance is 1% of its value at the surface.

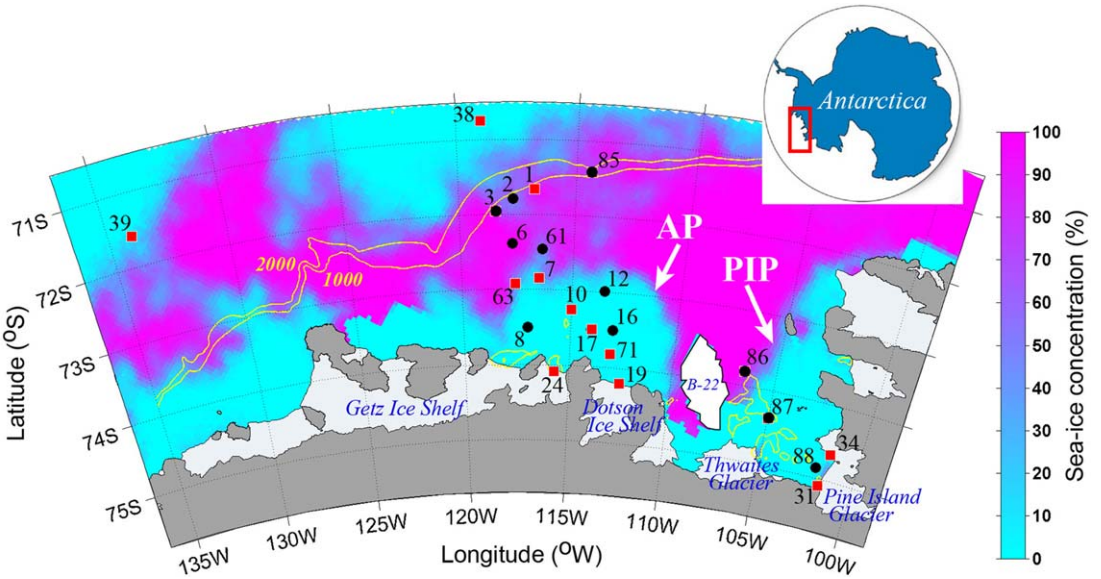

Fig. 1. Map of the study area, which covers the Amundsen Sea Polynya (ASP) and Pine Island Polynya (PIP). Red rectangles are the stations where Fe addition incubation experiments were conducted. Colors represent sea-ice concentration at the beginning of the cruise (10 February 2012–15 February 2012).

Due to high chlorophyll content in Antarctic polynyas, the incident solar light is attenuated rapidly by the water column and greatly reduces the effective PAR levels experienced by phytoplankton in the mixed layer which inevitably leads to light limitation of photosynthetic rates. To evaluate the impact of light limitation on the bloom development, we examined variations in the CRD in relation to the MLD. CRDs were calculated from the daily integrated irradiances at the surface and the measured light attenuation coefficients, according to Sverdrup's concept of CRD (Sverdrup 1953; Nelson and Smith 1991). Because changes in cloud cover and the resulting daily irradiances varied dramatically both temporarily and spatially, we used satellite-based climatological data for the month of February 2012 to retrieve the average daily irradiances for the ASP and PIP areas.

Water samples were collected from Niskin bottles at six standard depths. For measurements of chlorophyll *a* (Chl *a*) concentrations, seawater samples were filtered at a low vacuum through a 25 mm glass fiber filter (Whatman GF/F), then placed in 10 mL of 90% acetone in a conical tube. After extraction in the dark for 24 h, Chl *a* concentrations were measured using a Turner Designs fluorometer (Trilogy) calibrated with a purified Chl *a* standard solution, following the fluorometric method of Parsons et al. (1984). Microzooplankton grazing rates were estimated from the dilution experiments as described in Landry and Hassett (1982) and Yang et al. (2016).

Underway continuous measurements of variable fluorescence and fluorescence lifetimes of phytoplankton in the near-surface water layer (ca. 7 m depth) were conducted using mini-FIRe and Lifetime Fluorometers, respectively, as described in Lin et al. (2016).

Determination of phytoplankton photosynthetic parameters

Variable fluorescence was measured with a new miniaturized Fluorescence Induction and Relaxation System (called a mini-FIRe). This instrument is conceptually similar to the previous Fast Repetition Rate (FRR) and FIRe systems (Gorbunov and Falkowski 2005), but exhibits ca. 20 times better sensitivity and signal-to-noise, compared to its predecessors. Also, the mini-FIRe instrument employs excitation at multiple wavelengths (435 nm, 455 nm, 470 nm, 500 nm, 530 nm, and 590 nm, with 20 nm bandwidth of each channel) that allows for selective excitation of different functional groups of phytoplankton, as well as for spectrally resolved measurements of functional absorption cross-sections of PSII (σ_{PSII}). The peak excitation intensity at each wavelength is optimally adjusted to ensure full closure of PSII reaction centers and saturation of fluorescence within ca. 100 μs (i.e., a single photosynthetic turnover), which is critically important for accurate retrievals of functional cross sections and quantum yields (Gorbunov et al. 1999).

After collection from Niskin bottles, seawater samples were kept at in situ temperature and low light (ca. 10 μmol quanta m^{-2} s^{-1}) in transparent bottles. This low light adaptation (for ca. 60 min) was essential for recovery from photoinhibiton and non-photochemical quenching (Park et al. 2013). PSII parameters such as the minimal fluorescence yield (F_0; when all reaction centers are open), the maximal

fluorescence yield (F_m; all reaction centers are closed), and the quantum efficiency of PSII (F_v/F_m) were measured as described in Kolber et al. (1998). Quantum efficiency of photochemistry in PSII (F_v/F_m) was calculated as a ratio of variable fluorescence ($F_v = F_m - F_0$) to the maximum fluorescence (F_m). Fluorescence measurements were corrected for the blank signal recorded from filtered seawater (0.2 μm) as described in Bibby et al. (2008).

The rates of photosynthetic electron transport (ETR) were measured on samples collected from the mixed layer as a function of PAR, using a programmable Actinic Light Source integrated into the mini-FIRe instrument. The ETRs normalized per PSII reaction center were calculated as described in Gorbunov et al. (2000, 2001). The rate of photosynthetic electron transport (ETR) per PSII reaction center is given by

$$\mathrm{ETR} = E\sigma_{\mathrm{PSII}}'(\Delta F'/F_v') \quad (1)$$

where σ_{PSII}' is the functional absorption cross section of PSII and $\Delta F'/F_v'$ is the coefficient of photochemical quenching, which characterizes the fraction of open reaction centers at a given level of irradiance; the prime character indicates the measurements under ambient irradiance (E). When non-photochemical quenching is caused by thermal dissipation in the light-harvesting antennae, the Eq. 1 can be reduced to the following (Gorbunov et al. 2000):

$$\mathrm{ETR} = E\sigma_{\mathrm{PSII}}[(\Delta F'/F_m')/(F_v/F_m)] \quad (2)$$

where $\Delta F'/F_m'$ is the only irradiance-dependent variable. The photosynthetic rate as a function of irradiance can be described by the hyperbolic tangent equation (Jassby and Platt 1976):

$$\mathrm{ETR} = \mathrm{ETR}^{\max}\tanh(E/E_k) \quad (3)$$

where $\mathrm{ETR}^{\max}$ is the maximum rate achievable at saturating light and E_k is the light saturation parameter. Applying the model (3) to the experimental data ETR(E), we can calculate $\mathrm{ETR}^{\max}$ and E_k.

In order to deduce the photosynthetic rates in absolute units (i.e., electrons per second per reaction center), the cross sections must be measured for the same spectral quality as ambient irradiance. Here, we used blue (455 nm, with 20 nm half bandwidth) excitation and ambient light while recording P vs. E curves. Thereby, the retrieved maximum rates $\mathrm{ETR}^{\max}$, which are most critical for determining the photosynthetic rates integrated over the water-column, are independent on the spectral quality of measuring light. We further used these irradiance dependencies of photosynthetic rates in combination with vertical profiles of in situ PAR to reconstruct vertical profiles of photosynthetic rates over the mixed layer. We then calculated the averaged photosynthetic rates over the mixed layer and compare them with the potential maximum ($\mathrm{ETR}^{\max}$) in order to assess the extent of light limitation of photosynthesis.

Picosecond lifetime measurements

Picosecond fluorescence decay kinetics were measured using a custom-built lifetime fluorometer, called PicoLiF, as described in Kuzminov and Gorbunov (2016) and Lin et al. (2016). Both mini-FIRe and PicoLiF instruments are extremely sensitive and can accurately record fluorescence kinetics in ultra-low chlorophyll concentrations (down to 0.01 mg m^{-3}).

Measured kinetic curves were fitted using a sum of two or three exponential components that were convoluted with the instrumental response function (IRF) by employing a custom-built software package based on a TCSPFIT MATLAB routine, which uses a Nelder–Meade simplex algorithm (Enderlein and Erdmann 1997). The quality of the fit was evaluated from χ^2. The lifetimes given in this paper represent the average of the individual components:

$$\tau = \sum\nolimits_i f_i \cdot \tau_i \quad (4)$$

$$f_i = \frac{A_i \cdot \tau_i}{\sum_j f_j \cdot \tau_j} \quad (5)$$

where, τ_i, A_i, and f_i are the lifetime constants, amplitudes, and relative quantum yields of each component (Lakowicz 2006).

To produce fluorescence lifetime vs. F_v/F_m graphs, we applied a 300 × 300 grid to the study area (i.e., ASP and PIP). For each pixel of the grid we calculated a mean of F_v/F_m and lifetime.

Fe enrichment experiment

In order to assess the extent of Fe limitation of phytoplankton physiology, we conducted short-term Fe-enrichment experiments in on-deck incubators at 12 stations. The water samples were collected from the mixed layer (ca. 10 m depth) using trace-metal clean GO-FLO bottles and placed into 1 L polycarbonate bottles for incubations. All manipulations were conducted in a trace-metal clean plastic bubble which allowed us to avoid any contaminations. All surfaces of polycarbonate bottles were rigorously cleaned using trace-metal grade 1% HCl, followed by rinsing with deionized water (Milli-Q) and with ~ 50 L of seawater before sampling began. Once collected, the water was either enriched with 1 nM of iron ($FeCl_3$, Fluka) or left unamended for control. The incubations were conducted in on-deck incubators where the samples were maintained at in situ temperature and were exposed to ~ 10% of surface irradiance. After 3 d on-board incubations, changes in F_v/F_m and Chl *a* concentration were measured to document the response of phytoplankton to iron enrichment. Because the community structure did not change during the short-term incubations, the observed changes in F_v/F_m were indicative to iron-

Table 1. Oceanographic and biological data on water samples collected at stations. Temperature (°C), salinity (psu), and Chl *a* concentrations (mg m^{-3}) are surface values. F_v/F_m and σ_{PSII} at 455 nm ($Å^2$) are the values averaged over the mixed layer.

Region	Station	Date	Latitude (°S)	Longitude (°W)	Temperature	Salinity	MLD	Zeu	F_v/F_m	σ_{PSII}	Chl *a*	CRD
ASP	1	10 Feb	−71.66	−116.78	−1.81	33.57	27	27.9	0.329	477	3.21	34.2
	2	10 Feb	−71.79	−117.67	−1.78	33.47	33	25.6	0.267	439	3.03	31.3
	3	04 Mar	−71.95	−118.45	−1.79	33.64	25	-	0.383	529	0.14	-
	6	03 Mar	−72.39	−117.72	−1.80	33.62	26	24.7	0.429	497	3.29	30.3
	7	11 Feb	−72.85	−116.50	−1.68	33.58	22	22.8	0.362	455	3.41	27.9
	8	11 Feb	−73.50	−116.50	−1.57	33.46	41	20.9	0.355	448	3.84	25.6
	10	12 Feb	−73.25	−115.00	−1.12	33.54	40	14.8	0.340	428	2.95	18.1
	12	13 Feb	−72.99	−113.50	−1.60	33.64	18	18.1	0.301	427	4.46	22.2
	16	14 Feb	−73.50	−113.00	−1.38	33.64	31	18.1	0.307	441	6.20	22.2
	17	14 Feb	−73.50	−114.00	−1.24	33.48	37	17.6	0.277	432	5.72	21.5
	19	16 Feb	−74.20	−112.51	−1.67	33.77	16	41.8	0.341	455	0.81	51.2
	24	18 Feb	−74.08	−115.72	−0.83	33.73	30	28.2	0.353	425	1.74	34.6
	61	01 Mar	−72.46	−116.37	−1.78	33.54	28	30.7	0.401	509	2.82	37.6
	63	01 Mar	−72.93	−117.58	−1.74	33.38	26	15.3	0.428	488	2.00	18.8
	71	16 Feb	−73.82	−113.07	−1.29	33.68	57	14.8	0.297	436	4.89	18.1
	85	05 Mar	−71.42	−114.33	−1.82	33.44	41	26.3	0.285	558	0.39	32.2
PIP	31	24 Feb	−75.09	−101.76	−1.17	33.69	25	33.1	0.487	540	2.91	33.8
	34	25 Feb	−74.65	−101.53	−1.06	33.64	67	26.3	0.488	500	2.59	26.9
	86	27 Feb	−73.81	−106.54	−1.50	33.38	25	-	0.489	533	1.87	-
	87	22 Feb	−74.37	−105.00	−1.43	33.80	36	37.7	0.417	589	2.33	38.6
	88	23 Feb	−74.86	−102.10	−1.15	33.69	41	40.0	0.507	549	1.56	40.9
Open Sea	38	07 Mar	−70.45	−119.00	−1.13	33.29	20	-	-	-	-	-
	39	09 Mar	−71.58	−133.99	−1.32	33.35	44	15.5	0.243	585	0.35	-

induced changes in physiology rather than taxonomy (Suggett et al. 2009).

Remote sensing data

Level 3 monthly and 8-d composite regional maps of Chl *a* concentrations from Sea-viewing Wide Field-of-view Sensor (SeaWiFS) and Moderate-Resolution Imaging Spectroradiometer (MODIS) Aqua were obtained from the Goddard Space Flight Center. We analyzed 16 yr of austral summer (October–March) data sets, with the spatial resolution of approximately 9 km.

For sea-surface wind data, ERA-Interim data were downloaded from European Centre for Medium-Range Weather Forecasts (ECMWF; http://apps.ecmwf.int/datasets/). This is the latest global atmospheric reanalysis produced by the ECMWF, with the spatial resolution of 1/4 degree. Seventeen-year summer mean (December–March) data sets were used for comparison of the two regions (ASP and PIP, respectively).

Global ocean color data were also used to assess the cloud coverage and the effective daily levels of PAR at the ocean surface. This data has been constructed from multi ocean color sensors such as SeaWiFS, MODIS, Medium Resolution Imaging Spectrometer (MERIS), and Visible Infrared Imaging Radiometer Suite (VIIRS), downloaded from the Globcolour site (http://hermes.acri.fr). We used 16 yr summer mean (December–March) data sets for comparison.

We also used daily SSMIS F-17 microwave remote sensing data, retrieved from the University of Bremen (http://www.iup.uni-bremen.de:8084/ssmis/) for sea ice coverage during the study. These data were processed using a Bootstrap algorithm with 25 km^2 resolution.

Results

Two polynyas (ASP and PIP) and three ice shelves (Dotson, Getz, and Pine Island Glacier (PIG)) belong to our study area (Fig. 1). The study area was divided into three regions geographically as follows: (1) ASP and surrounding seasonal ice zone (16 stations), (2) PIP (5 stations), and (3) open sea (Sta. 38 and 39).

Seasonal dynamics of phytoplankton biomass in the Amundsen polynyas as retrieved from ocean color remote sensing

During the cruise, in situ measured surface Chl *a* concentrations ranged from 0.14 mg m^{-3} to 6.20 mg m^{-3} with a maximum concentration observed in the ASP center (Sta. 16; Table 1). These high chlorophyll concentrations in this polynya are also supported by satellite-based ocean color data. Figure 2 shows the 16 yr (1997–2013) composite of

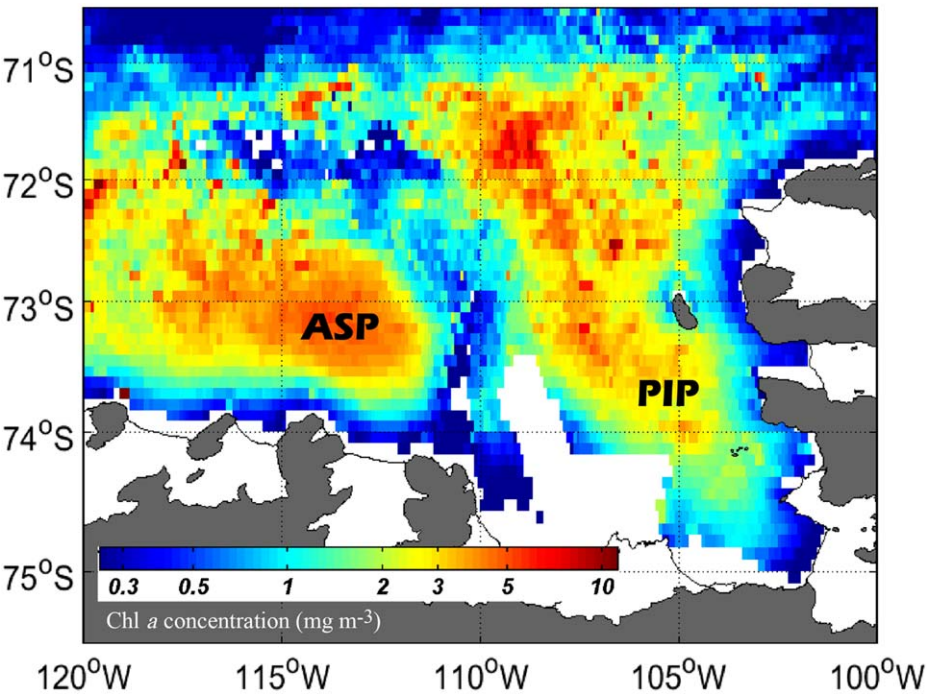

Fig. 2. Sixteen years (1997–2013) composite map of Chl *a* concentrations in the Amundsen Sea in austral summer (October–March), based on remotely sensed ocean color data.

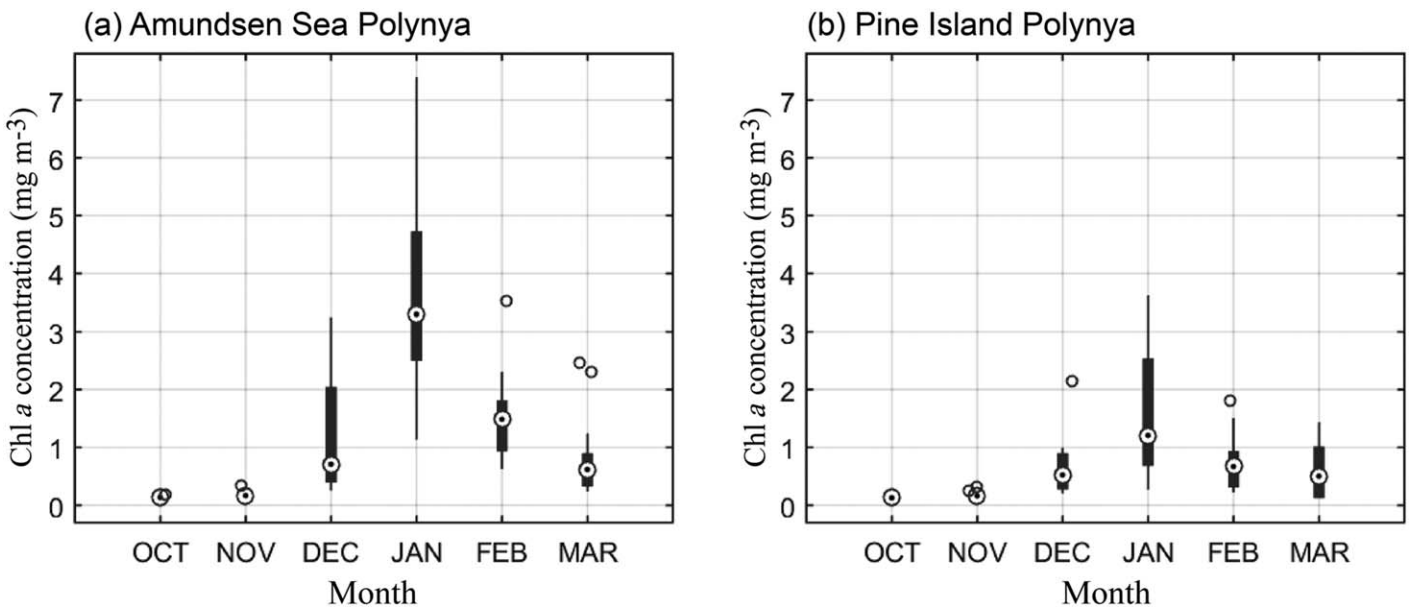

Fig. 3. Temporal evolution of Chl *a* concentrations in (**a**) the Amundsen Sea Polynya, and (**b**) Pine Island Polynya during the austral summer. The values were averaged over the period of 16 yr (1997–2013). Boxplots are distributions of interannual variations for each month. The inner circles in the boxplots represent the median. The boxes delimit the 25th and 75th percentiles, and outer circles indicate outliers.

satellite Chl *a* concentrations in the Amundsen Sea in austral summer. The summer mean (October–March) Chl *a* concentration in the ASP center was more than 5 mg m^{-3}. In contrast, the maximum value of the summer mean Chl *a* concentration in the PIP center was ca. 3 mg m^{-3}. The phytoplankton bloom starts in December in both polynyas and peaks in January (Fig. 3). The year-to-year variations are also substantial in both polynyas, especially in December and

January for the ASP and in January and March for the PIP. Moreover, satellite-based ocean color data over a 10 yr period reveals that peak chlorophyll concentrations in the ASP are about two times higher than those in the PIP (Figs. 2, 3). The phytoplankton bloom in both polynyas was declining during our study (i.e., mid February to mid March 2012).

Spatial distributions of phytoplankton physiological status in two polynyas

Surface water properties such as temperature, salinity, MLD, and euphotic depth as well as phytoplankton biomass and physiological parameters are shown in Fig. 4. The sea surface temperature and salinity were similar between the two polynyas (difference < 0.3°C and < 0.1 psu, respectively). Freshening of surface waters by sea ice melt strengthen stratification of the upper water column, which resulted in a shallower MLD in the marginal ice zone as compared with the central polynya and areas near the ice shelves. The maximum quantum efficiencies of PSII (F_v/F_m) in the near-surface phytoplankton were highest in the PIP, moderate around the marginal ice zone of the ASP, and lowest in the central part of the ASP. Overall, F_v/F_m decreased in regions with highest chlorophyll concentrations.

To determine the role of light limitation in controlling the bloom development, we analyzed variations in CRDs in relation to MLDs. MLDs in the ASP varied from 18 m (Sta. 12) to 57 m (Sta. 71), with a mean of 31.1 m. MLDs in the PIP ranged from 25 m to 67 m, with a mean of 38.8 m. In the ASP area, CRDs varied from 18 m to 51 m, with a mean of 28.4 m. In the PIP, CRDs varied from 27 m to 41 m, with a mean of 35 m (Table 1). In both ASP and PIP, MLD values closely approached or even exceeded CRD values, imposing light limitation on blooms in both regions.

Vertical distributions of F_v/F_m, σ_{PSII}, and Chl *a* concentration (averaged over a total of 16 and 5 stations in the ASP and PIP, respectively) are shown in Fig. 5. Generally, the F_v/F_m increased with depth in the upper 70 m of the water column, but Chl *a* concentrations were highest within the upper 20 m and decreased with depth in both polynyas. The averaged surface values of F_v/F_m were low (0.34 ± 0.06) in the ASP and relatively high (0.48 ± 0.03) in the PIP. The F_v/F_m was also very low (ca. 0.24) at open sea stations. On the other hand, the averaged surface Chl *a* concentrations were higher in the ASP (3.05 ± 1.77 mg m^{-3}) than in the PIP (2.25 ± 0.54 mg m^{-3}). The surface Chl *a* concentration was lowest at open sea stations (ca. 0.35 mg m^{-3}). In general, the values of σ_{PSII} in the blue spectral region (at 455 nm) did not vary with depth, and were consistently higher in the PIP (average of 542 Å^2) and open sea stations (567 Å^2) than in the ASP (465 Å^2).

High-resolution horizontal distributions of F_v/F_m, which were reconstructed from underway measurements, are shown in Fig. 6a. The highest subsurface values of F_v/F_m (> 0.40) were observed in the northeast marginal ice zone and in the PIP, in the vicinity of PIG. In contrast, the lowest F_v/F_m values (0.19–0.32) were observed in the ASP. In the central ASP (with the highest chlorophyll concentration) F_v/F_m was as low as ca. 0.2. F_v/F_m was also about 0.25 in front of the Dotson and Getz ice shelves. On average, the F_v/F_m values were $> 25\%$ lower in the ASP than in the PIP.

Figure 6b shows horizontal distributions of chlorophyll fluorescence lifetimes in the ASP and PIP, reconstructed from continuous underway measurements. These lifetimes were maximal ($\sim$ 2 ns) in the open ocean and minimal (0.7–1.3 ns) in the PIP region. The distributions of lifetimes across the ASP showed a dramatic ($\sim$ 3-fold) variability (from 0.7 ns to 2.1 ns, Fig. 6c). The central part of ASP was characterized by exceptionally long lifetimes (1.1–1.4 ns). The area in front of the Dotson and Getz ice shelves with lower chlorophyll concentrations was characterized by relatively fast fluorescence lifetimes, which was distinct from the central part of ASP. Extremely long lifetimes were observed in the low chlorophyll region on the border with the open ocean (Fig. 6). Overall, there was an inverse relationship between fluorescence lifetimes and F_v/F_m (panels C and D in Fig. 6, *see* also Fig. 7). Because the fluorescence lifetime is directly proportional to the quantum yield of fluorescence (Lin et al. 2016), this inverse relationship indicates that reduction in photosynthetic efficiency increases dissipation of absorbed energy via fluorescence emission.

In vitro Fe enrichment experiments

After short term incubations with iron addition, F_v/F_m values generally increased as compared to the control treatment (Fig. 8). The biggest ($> 10\%$) increases in F_v/F_m were observed at Sta. 17, 71, 19, 24, and 38 in the ASP and in the open ocean (Fig. 1). Changes in chlorophyll concentrations were small and not significant. This pattern is consistent with previous Fe enrichment experiments in the Southern Ocean and reflects a slow response in biomass at low temperatures (Gervais et al. 2002; Coale et al. 2004). In contrast to ASP, iron enrichment did not change F_v/F_m in samples collected in the PIP and the seasonal ice zone surrounding the ASP.

Discussion

Variability in physiological parameters of phytoplankton in relation to Fe stress

Our combination of variable fluorescence analysis, fluorescence lifetime measurements, and short-term incubation experiments provided unambiguous evidence on the striking differences in phytoplankton photophysiological status and iron stress between the two largest Amundsen Sea polynyas. These analyses revealed that phytoplankton in the ASP show signatures of Fe limitation in the late summer, while that in the PIP remain Fe-replete. Nevertheless, chlorophyll biomass in the Fe-replete PIP remained 30–50% lower than that in Fe-limited ASP, suggesting that the paucity of Fe is not the

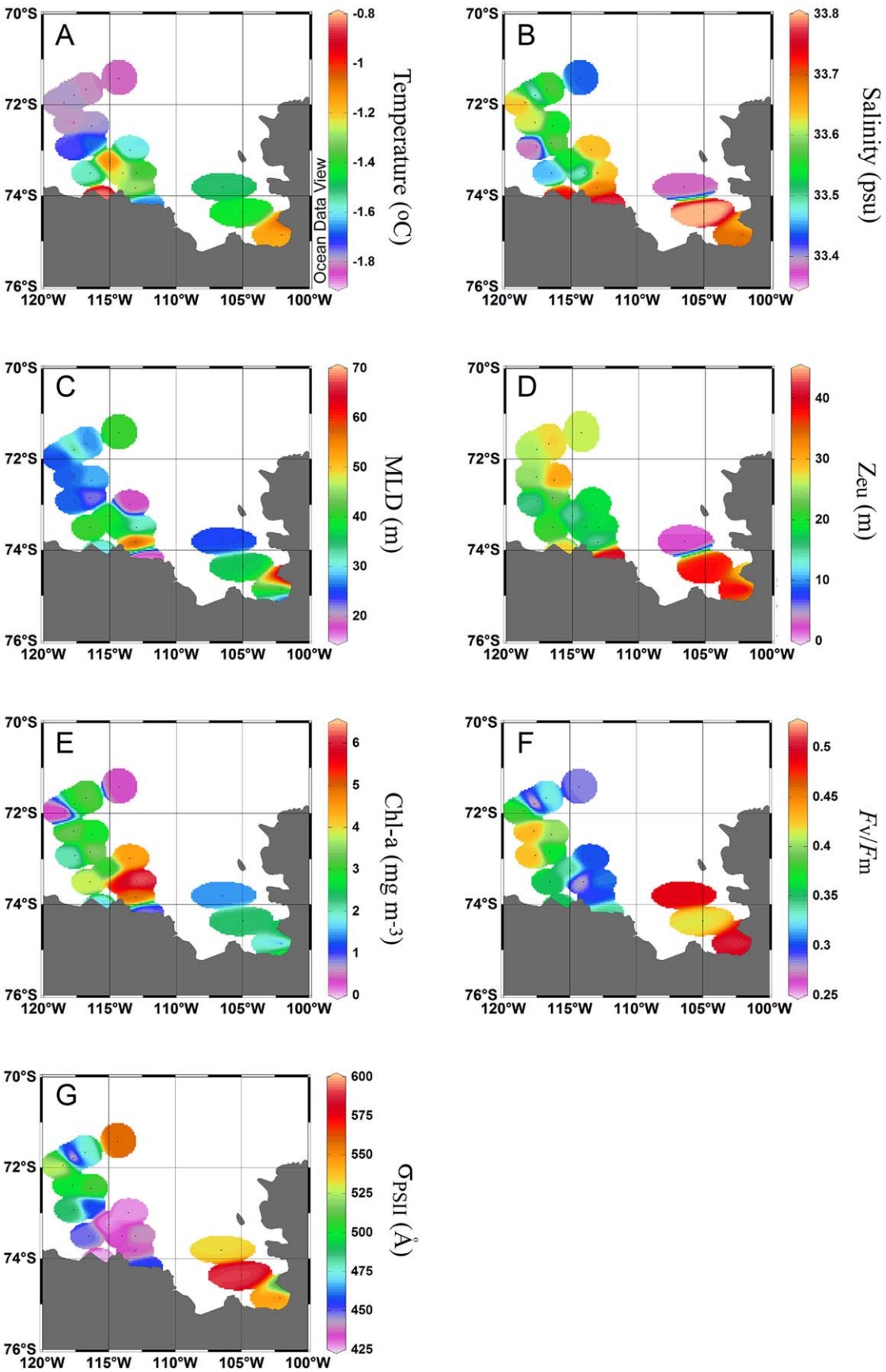

Fig. 4. Surface water properties across the two polynyas in the Amundsen Sea in the late summer 2012. (**a**) Sea surface temperature, (**b**) Sea surface salinity, (**c**) Mixed layer depth, (**d**) Euphotic depth, (**e**) Chl a concentration, (**f**) Quantum efficiency of photochemistry in PSII, and (**g**) Functional absorption cross-sections of PSII.

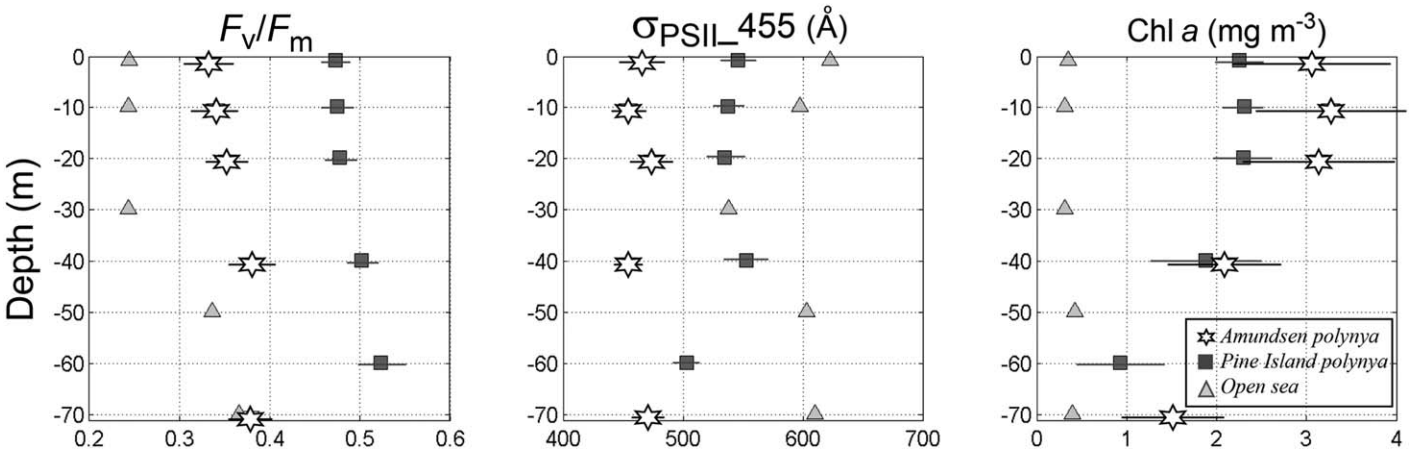

Fig. 5. Vertical profiles of F_v/F_m, the functional absorption cross section of PSII (σ_{PSII}) at 455 nm, and Chl *a* concentration in the Amundsen Sea Polynya, Pine Island Polynya (16 and 5 stations averaged, respectively), and the open sea area. Horizontal lines indicate the range of variability (i.e., standard deviations) in respective parameters in each region.

main limiting factor that controls the magnitude of the bloom in the Amundsen Sea. Below, we quantitatively examine physical, chemical, and biological controls that may contribute to the observed difference between ASP and PIP.

The first biophysical evidence of iron stress comes from our documented horizontal variability in the quantum yields of photochemistry in PSII (F_v/F_m). The maximum values of F_v/F_m observed in iron-enriched waters of the Southern Ocean are about 0.55 (Gervais et al. 2002; Coale et al. 2004). Our measured values of F_v/F_m in the PIP (0.48 ± 0.03, Fig. 5; Table 1) were very close to this maximum, clearly suggesting that phytoplankton were not iron limited in this region. In contrast, F_v/F_m values in the ASP (0.34 ± 0.06) were ca. 40% lower and similar to those observed previously in other iron-limited regions of the Southern Ocean (Hopkinson et al. 2007; Peloquin and Smith 2007). These values are comparable with the F_v/F_m values (< 0.35) observed in the central ASP in the early summer (Alderkamp et al. 2015). Our study was conducted in the late austral summer when iron limitation was expected to be critical. Nevertheless, our data suggest that phytoplankton physiology was significantly iron-limited only in the ASP, while phytoplankton remained iron-replete in the PIP region.

The other environmental factor that could potentially reduce F_v/F_m is photoinhibition (Falkowski et al. 2004). However, because we measured F_v/F_m in low-light acclimated samples, the effect of photoinhibition was alleviated (Park et al. 2013).

The functional absorption cross sections of PSII, σ_{PSII}(455 nm), in near surface phytoplankton were significantly ($\sim$ 20%, $p < 0.05$) smaller in the Fe-limited ASP than in the PIP (on average, 465 Å^2 vs. 542 Å^2, respectively). This difference cannot be explained by Fe limitation alone. Fe limitation usually increases cross-sections of PSII (Vassiliev et al. 1995). The cross-sections of PSII vary between species and variations in σ_{PSII} may also reflect changes in taxonomic composition (Suggett et al. 2009) and cell size distribution (Gorbunov et al. 1999). For example, Antarctic diatoms tend to have higher cross sections then *Phaeocystis antarctica* (Smith et al. 2013). During our study, *P. antarctica* was slightly more abundant in the ASP, but not significantly different from that in the PIP to fully explain the observed difference in cross-sections. Alternatively, the reduced cross-sections of PSII in the ASP may reflect that phytoplankton in this polynya were exposed and became acclimated to higher light regimes than in the PIP region.

The second, biophysical based evidence of iron limitation of phytoplankton photosynthesis in the ASP comes from our high spatial resolution measurements of chlorophyll fluorescence lifetimes. Fluorescence lifetimes are directly proportional to the quantum yields of fluorescence (Lakowicz 2006) and are strongly affected by phytoplankton physiological state. Biophysical models predict that in a dark-adapted state, there is an inverse relation between the quantum yield of photochemistry and that of fluorescence (Lin et al. 2016). Under optimal conditions, when all the reaction centers are active and open, the fluorescence lifetimes are minimal ($\sim$ 0.5–0.6 ns). When the reaction centers are closed (i.e., photochemistry is nil), the lifetimes increase to 1.5–1.8 ns (Kuzminov and Gorbunov 2016). Nutrient stress also leads to an increase in fluorescence lifetimes due to an increase in the fraction of inactive reaction centers and the presence of uncoupled light-harvesting antennae (Vassiliev et al. 1995; Behrenfeld et al. 2006; Schrader et al. 2011; Lin et al. 2016).

The shortest fluorescence lifetimes (0.7–1.3 ns) were observed in the PIP (Fig. 6b,d) where F_v/F_m values were maximal, indicating the absence of iron stress in this region. In the ASP, the variability of the fluorescence lifetimes was substantially greater (0.7–2.1 ns) with a significant portion of

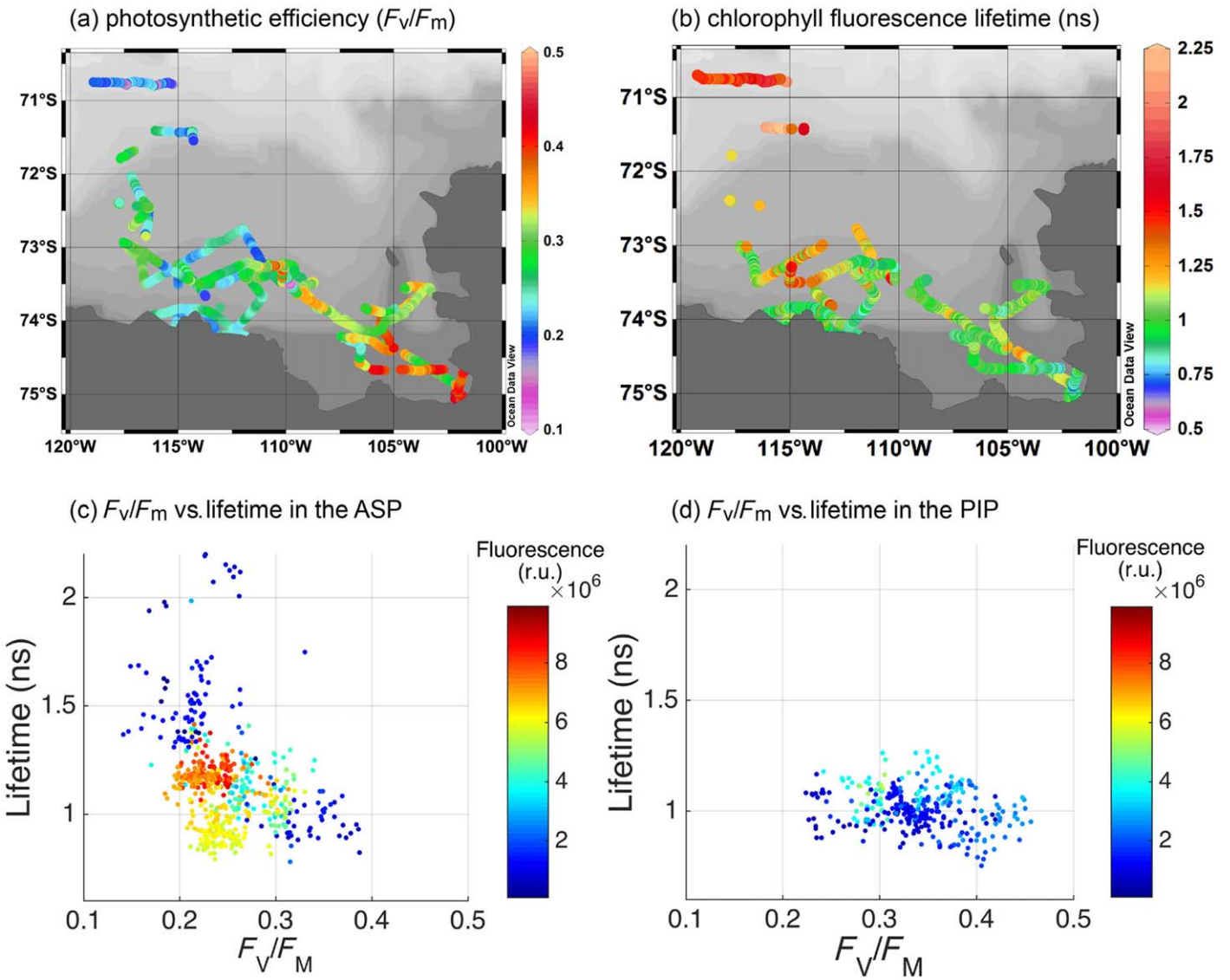

Fig. 6. High spatial resolution horizontal distributions of (**a**) the phytoplankton photosynthetic efficiency (F_v/F_m), (**b**) chlorophyll fluorescence lifetime (ns), (**c**) relationship between F_v/F_m values and chlorophyll fluorescence lifetimes in the ASP, and (**d**) relationship between F_v/F_m values and chlorophyll fluorescence lifetimes in the PIP reconstructed based on continuous underway measurements.

lifetimes > 1.2 ns, indicating a large pool of non-functional reaction centers and possibly detached antenna complexes. Extremely long lifetimes (> 2 ns) were also observed in the equatorial Pacific Ocean (Lin et al. 2016), a region exposed to persistent iron limitation.

In order to estimate the portion of detached antenna complexes we modeled dependence between F_v/F_m and fluorescence lifetimes, when 0–40% of the antenna complexes are detached (Fig. 7). We assumed an inverse relationship between F_v/F_m and the quantum of fluorescence (Butler 1978; Lin et al. 2016) and used the following fluorescence lifetimes criteria: 0.5 ns for fully open reaction center, 1.5 ns for fully closed reaction center, and 4 ns for detached antenna complexes. The presence of detached antenna complexes would ultimately lead to longer fluorescence lifetimes, as compared to those predicted by the Butler's model, and these lifetimes may exceed the values observed for fully closed reaction center (~ 1.5 ns) (Fig. 7). From Fig. 7 it could be estimated that Fe-limited regions of ASP have less than 25% of the antenna complexes detached. In comparison, iron limited regions in the open ocean exhibit extremely long fluorescence lifetimes (> 1.5 ns), indicating a substantial portion (up to 40%) of detached antenna complexes.

Generally, chlorophyll fluorescence lifetimes in our study increased in the areas with highest chlorophyll concentrations. For instance, in the central part of ASP, where

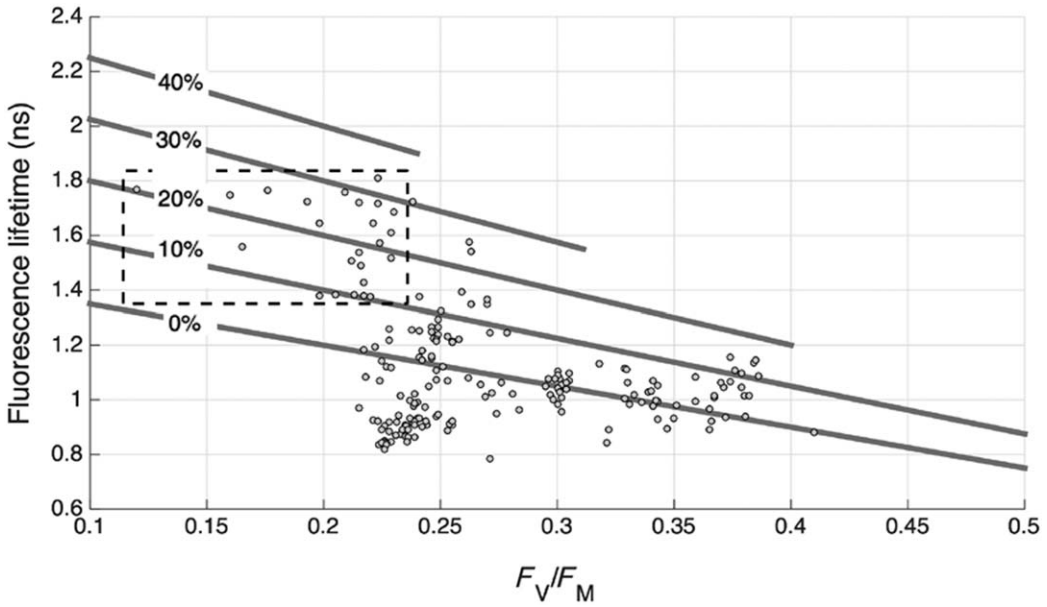

Fig. 7. Relationship between fluorescence lifetimes and F_v/F_m. In order to eliminate the effect of photoinhibition only night time values of F_v/F_m and fluorescence lifetimes were used. Solid gray line (with 0% mark) is the theoretical dependence between the fluorescence lifetime and F_v/F_m given the following dependence: $F_v/F_m = (\tau_m\text{-}\tau)/\tau_m$, where τ_m is estimated to be 1.5 ns (Kuzminov and Gorbunov 2016), and τ varies from 0.5 ns to 1.5 ns. Solid light gray line (with 10–40% marks) is the modeled dependence between F_v/F_m and τ, when 10–40% of the antenna are detached from the photosynthetic reaction center and have fluorescence lifetime of 4 ns. Box with dashed outline contains data points measured in the open ocean.

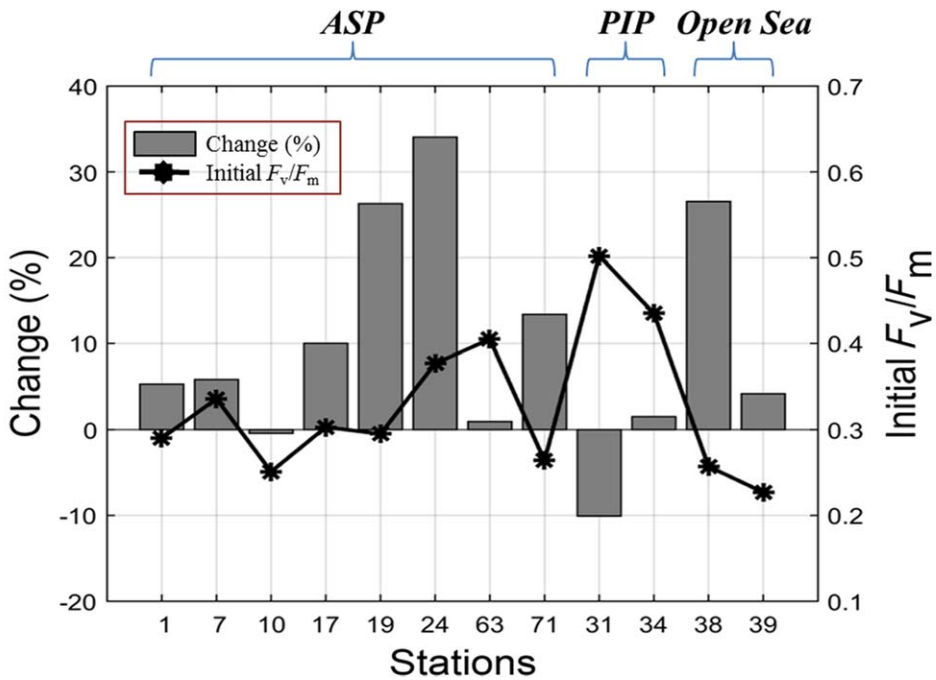

Fig. 8. Effect of iron enrichment on phytoplankton photosynthetic efficiency (F_v/F_m), based on short-term incubation experiments. The values on left side of Y-axis are a change (in %) relative to control (bars), and the values on right side of Y-axis are initial F_v/F_m on site (stars).

chlorophyll concentrations exceeded 5 mg m^{-3}, the lifetimes were > 1.2 ns. This may indicate that at high standing stock (> 5 mg m^{-3}) Fe fluxes are not sufficient to maintain maximum photosynthetic rates in the ASP. Therefore, paucity of iron could limit phytoplankton photophysiology mostly at the late stage of bloom development in the ASP, but

that iron limitation is not responsible for the relatively low productivity in the PIP.

The above-described biophysical signatures of iron limitation in the ASP are further supported by our iron enrichment experiments in on-deck incubators. If phytoplankton are Fe-limited, then Fe addition would increase photosynthetic efficiency and, ultimately, growth (Olson et al. 2000; Behrenfeld et al. 2006). Although F_v/F_m may be affected by the taxonomic composition of phytoplankton (Suggett et al. 2009), there is, in general, a good correlation between the in situ F_v/F_m values and the subsequent response to iron addition in the Southern Ocean (Hopkinson et al. 2007). Other reports also showed that the F_v/F_m values were inversely correlated with the availability of iron in the Southern Ocean (Olson et al. 2000; Boyd and Abraham 2001). Our short term iron enrichment incubations (Fig. 8) clearly suggest that the ASP was iron-limited, but the PIP was not.

Physical controls of phytoplankton growth

Our analysis of the multi-year ocean color data showed that the dynamics and spatial patterns of phytoplankton bloom in both polynyas were similar (Fig. 3), but that the ASP exhibited consistently higher chlorophyll biomass than the PIP. This trend is further supported by our in situ measurements, including fluorescence-based estimates of chlorophyll biomass and standard chemical measurements of chlorophyll concentrations in the water column. Analysis of vertical profiles of chlorophyll concentrations revealed that the water-column integrated biomass in the ASP was ca. 30% higher than that in the PIP (118 ± 74 mg m^{-2} vs. 89 ± 50 mg m^{-2}, respectively). Iron limitation (e.g., in ASP) leads to a marked reduction in chlorophyll content (i.e., chlorosis) in a plant cell, thus increasing the C/Chl *a* ratio (Greene et al. 1991; Coale et al. 2004). For instance, the C/Chl *a* ratio in Fe-limited areas of the ASP is significantly higher than that in PIP (Alderkamp et al. 2012*b*). For this reason, the difference in carbon biomass between the Fe-limited ASP and the Fe-replete PIP should be even greater than the difference in chlorophyll biomass.

The remotely sensed data on sea-ice concentration showed that both ASP and PIP, in general, were opened from the southeast in the spring and expanded to the northwest during the summer. As a consequence, the phytoplankton bloom peaked in early January in the eastern parts of the polynyas and in late January in the western parts. Although the ASP was opened for ca. 10 d longer than the PIP, the peak timing and spatial patterns of phytoplankton bloom were similar in both polynyas. Other physical characteristics such as temperature, salinity, and MLD were also very similar between these two polynyas (Fig. 4). Persistently lower biomass of the PIP appears to contradict high Fe availability and the absence of Fe stress in this area. Such apparent paradox would not have been observed if Fe availability were the main control of phytoplankton blooms in the Amundsen Sea. Our data analysis clearly rejects Hypothesis 1 (as put forward in the Introduction).

In the Southern Ocean, concentrations of macronutrients in the euphotic zone are at the highest levels observable in the global oceans and rarely become depleted even at the peak of seasonal blooms (Arrigo et al. 2008). During our study, the macronutrients were abundant in the upper water column and not significantly ($p > 0.1$) different between the two polynyas. For instance, nitrate + nitrite was 18.4 ± 4.9 μM L^{-1} and 18.7 ± 3.0 μM L^{-1} in ASP and PIP, respectively; phosphate was 1.54 ± 0.26 μM L^{-1} and 1.52 ± 0.12 μM L^{-1} in ASP and PIP, respectively; silicate was 74.3 ± 6.4 μM L^{-1} and 60.7 ± 3.6 μM L^{-1} in ASP and PIP, respectively.

Grazing by microzooplankton is an important top-down control of primary production, which is mostly pronounced at the late stages of bloom development in the Southern Ocean. To examine whether the grazing pressure could contribute to the observed difference in phytoplankton biomass between ASP and PIP, we estimated the grazing rates from dilution experiments, as described in Landry and Hassett (1982). These experiments showed no significant difference ($p > 0.1$) in grazing pressure between these two polynyas. For instance, microzooplankton grazers consumed $76\% \pm 23\%$ and $80\% \pm 34\%$ of daily gross primary production in the ASP and PIP, respectively. Therefore, our data clearly suggest that macronutrients and grazing pressures were similar between ASP and PIP and, hence, these factors could not explain the observed difference in bloom magnitude between these two areas.

Light limitation and low temperature have been recognized as limiting factors of primary productivity in the Southern Ocean (Holm-Hansen and Mitchell 1991; Mitchell and Holm-Hansen 1991). Light regimes in polar regions vary dramatically with season, but in the summer the maximum daily integrated irradiance levels at the surface are as high as in the tropics (Campbell and Aarup 1989). However, wind-driven vertical mixing and cloud cover may markedly reduce the effective irradiance levels in the water column. Strong attenuation of incident light by chlorophyll rich waters further reduces the effective light levels in the mixed layer (Schofield et al. 2015). During our study, the mixed layer was slightly (ca. 25%) shallower and thus more favorable for bloom development in the ASP than in the PIP (31.1 m vs. 38.8 m, respectively), but the light conditions experienced by phytoplankton within the upper water column were similar because of greater light attenuation coefficients in the ASP.

To quantify the impact of light limitation on the bloom development, we examined variations in the CRD in relation to the MLD. This analysis revealed that in both ASP and PIP, MLD values closely approached or even exceeded CRD values, indicating a condition that imposes severe light limitation (Sverdrup 1953) on bloom development in both regions.

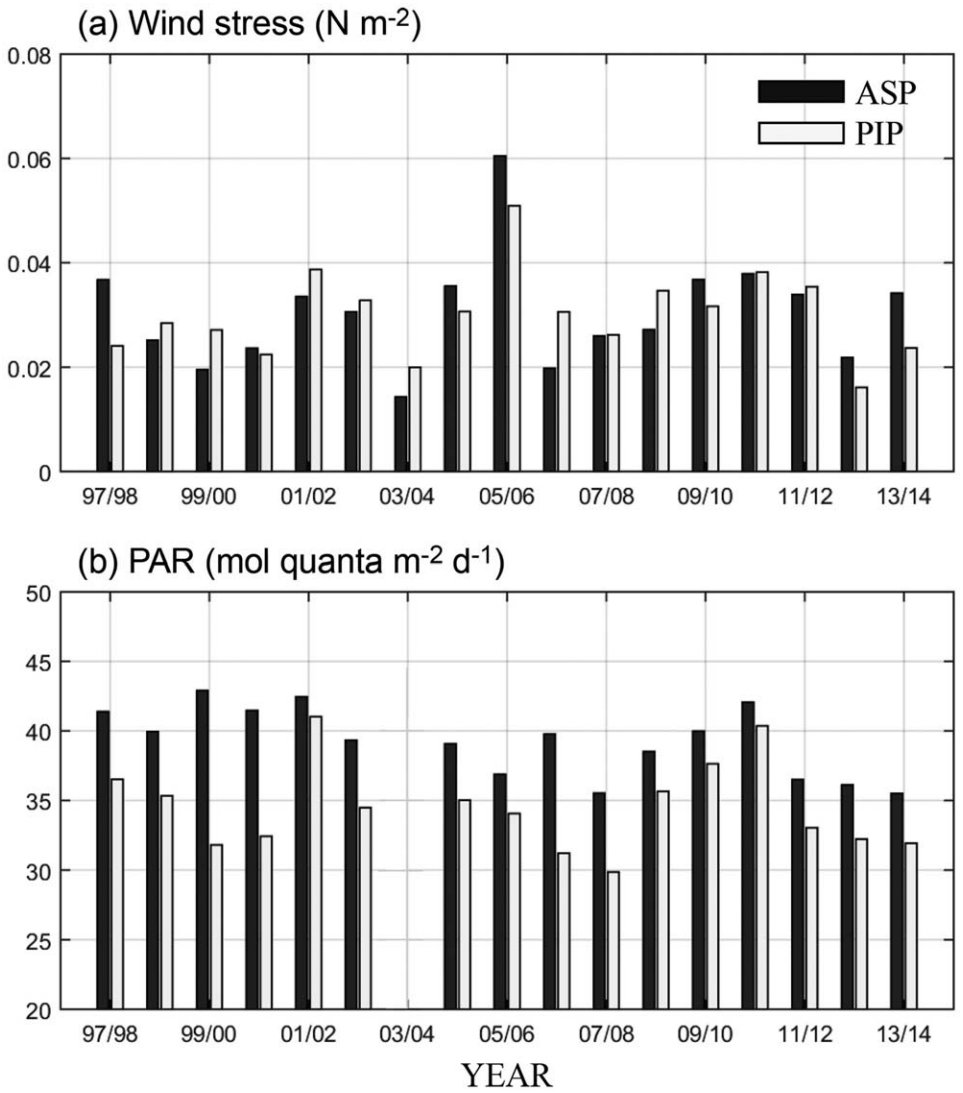

Fig. 9. Comparison of (**a**) ECMWF wind stress (N m^{-2}), and (**b**) remotely sensed Photosynthetically Available Radiation (PAR; mol quanta m^{-2} d^{-1}) between ASP and PIP. Seventeen years (1997–2014; 1 yr missing for PAR) data were used for analysis. All data represent December–January mean.

Further evidence of severe light limitation of primary productivity comes from our measurements of photosynthetic rates in the mixed layer as a function of PAR, in combination with the vertical profiles of PAR. This biophysical analysis revealed that even under clear skies $\sim$ 73% of phytoplankton in the mixed layer were exposed to PAR levels below the saturating light intensity ($E_k \sim 224$ μM m^{-2} s^{-1}, $n = 17$) and thus were light-limited. Under cloudy skies, $>91\%$ of phytoplankton in the mixed layer were light-limited. The combined analysis of P-vs.-E measurements, climatological PAR data for the Amundsen Sea, and in situ light attenuation coefficients showed that, on average, 97–98% of phytoplankton in the mixed layer were exposed to light-limiting irradiances. Because of severe light limitation, the average photosynthetic electron transport rates (ETR $= 25 \pm 19$ e/s per PSII reaction center) in the mixed layer were almost an order of magnitude lower than their potential maximum ($ETR^{max} = 200 \pm 67$ e/s per reaction center). For comparison, reduction in the photosynthetic rates in the ASP due to Fe limitation (based on F_v/F_m measurements) was only $\sim$ 40%.

In order to elucidate whether there is a difference in wind-driven vertical mixing regimes between the two polynyas on longer temporal scales, we further examined the 17-yr satellite-based record of wind velocities and wind stress curl in the Amundsen Sea. This analysis revealed no significant difference in the seasonally averaged wind velocities between the ASP and PIP (Fig. 9a). The values of wind stress ranged from 0.014 N m^{-2} to 0.061 N m^{-2} (with a mean of 0.030 ± 0.011 N m^{-2}) in the ASP and from 0.016 N m^{-2} to 0.051 N m^{-2} (0.030 ± 0.009 N m^{-2}) in the PIP. The wind stress curl was higher in PIP, which may stimulate upwelling

and bring more Fe to already Fe-rich surface waters in this region, with no effect on primary productivity. Clearly, the 17-yr record revealed no difference in the wind stress between the two polynyas that can affect the light regimes experienced by phytoplankton.

In contrast to the wind stress data, the season-averaged sea surface irradiance levels were markedly higher in the ASP than in the PIP (Fig. 9b). The values ranged from 35.5 to 42.9 mole quanta m^{-2} d^{-1} (with a mean of 39.3 ± 2.45 mole quanta m^{-2} d^{-1}) in the ASP and from 29.9 to 41.0 mole quanta m^{-2} d^{-1} (34.5 ± 3.18 mole quanta m^{-2} d^{-1}) in the PIP. This difference was clearly observed each year, in correspondence with higher biomass accumulation in the ASP. Therefore, irradiance data further supports our Hypothesis 2 (as put in the Introduction) that light availability rather than Fe is the main driver of phytoplankton bloom dynamics in the Amundsen Sea polynyas.

Our study is the first quantitative comparison of two major bottom-up controls (iron and light) of primary productivity in the Amundsen Sea. Our analyses revealed striking differences in both iron stress and irradiance regimes experienced by phytoplankton between the two largest Amundsen Sea polynyas. The inference about variations in iron stress is supported by four lines of evidence, including high spatial resolution underway measurements of variable fluorescence, vertical profiles of variable fluorescence, chlorophyll fluorescence lifetime measurements, and short-term iron enrichment experiments. These biophysical analyses revealed that phytoplankton physiology was iron-limited in the ASP, but remained iron-replete in the PIP in late austral summer. These results corroborate previous observations of exceptionally high Fe concentrations (> 1.2 nM) in the upper water column in the PIP (Gerringa et al. 2012) and low Fe in the ASP (< 0.3 nM) (Gerringa et al. 2012; Sherrell et al. 2015). In spite of enhanced Fe availability, biomass in the PIP remained $\sim$ 30–50% lower than that in the Fe-stressed ASP, suggesting that iron is not the main limiting factor of the phytoplankton bloom. Long-term satellite-based climatology records revealed that the ASP is exposed to significantly higher solar irradiance levels throughout the summer season, as compared to the PIP region, suggesting that light availability is the main control of phytoplankton bloom dynamics in the Amundsen Sea. These data have an important implication for predicting the future impact of climate variations on the primary production in Antarctic biological hotspots. Our analysis suggests that, in spite of what was previously thought, higher Fe availability (e.g., due to higher melting rates of ice sheets) would not necessarily increase primary productivity in this region. Instead, the increase in productivity might be achieved by relief from light limitation. Therefore, understanding how environmental and climate change may influence the light fields in polar hot spots is particularly critical.

References

Alderkamp, A.-C., G. Kulk, A. G. Buma, R. J. Visser, G. L. Van Dijken, M. M. Mills, and K. R. Arrigo. 2012*a*. The effect of iron limitation on the photophysiology of Phaeocystis antarctica (Prymnesiophyceae) and Fragilariopsis cylindrus (Bacillariophyceae) under dynamic irradiance. J. Phycol. **48**: 45–59. doi:10.1111/j.1529-8817.2011.01098.x

Alderkamp, A.-C., and others. 2012*b*. Iron from melting glaciers fuels phytoplankton blooms in the Amundsen Sea (Southern Ocean): Phytoplankton characteristics and productivity. Deep-Sea Res. Part II **71–76**: 32–48. doi:10.1016/j.dsr2.2012.03.005

Alderkamp, A.-C., and others. 2015. Fe availability drives phytoplankton photosynthesis rates during spring bloom in the Amundsen Sea Polynya, Antarctica. Elementa **3**: 000043. doi:10.12952/journal.elementa.000043

Arrigo, K. R., and G. L. Van Dijken. 2003. Phytoplankton dynamics within 37 Antarctic coastal polynya systems. J. Geophys. Res. **108**: 3271. doi:10.1029/2002JC001739

Arrigo, K. R., L. Van Dijken, and S. Bushinsky. 2008. Primary production in the Southern Ocean, 1997-2006. J. Geophys. Res. **113**: C08004. doi:10.1029/2007JC004551

Arrigo, K. R., E. Lowry, and G. L. Van Dijken. 2012. Annual changes in sea ice and phytoplankton in polynyas of the Amundsen Sea, Antarctica. Deep-Sea Res. Part II **71–76**: 5–15. doi:10.1016/j.dsr2.2012.03.006

Behrenfeld, M. J., K. Worthington, R. M. Sherrell, F. P. Chavez, P. Strutton, M. McPhaden, and D. M. Shea. 2006. Controls on tropical Pacific Ocean productivity revealed through nutrient stress diagnostics. Nature **442**: 1025–1028. doi:10.1038/nature05083

Bibby, T. S., Y. Gorbunov, K. W. Wyman, and P. G. Falkowski. 2008. Photosynthetic community responses to upwelling in mesoscale eddies in the subtropical North Atlantic and Pacific Oceans. Deep-Sea Res. Part II **55**: 1310–1320. doi:10.1016/j.dsr2.2008.01.014

Boyd, P. W., and E. R. Abraham. 2001. Iron-mediated changes in phytoplankton photosynthetic competence during SOIREE. Deep-Sea Res. II **48**: 2529–2550. doi:10.1016/S0967-0645(01)00007-8

Butler, W. L. 1978. Energy distribution in the photochemical apparatus of photosynthesis. Annu. Rev. Plant Physiol. **29**: 345–378. doi:10.1146/annurev.pp.29.060178.002021

Campbell, J. W., and T. Aarup. 1989. Photosynthetically available radiation at high-latitudes. Limnol. Oceanogr. **34**: 1490–1499. doi:10.4319/lo.1989.34.8.1490

Coale, K. H., and others. 2004. Southern Ocean Iron Enrichment Experiment: Carbon cycling in high- and low-Si waters. Science **304**: 408–414. doi:10.1126/science.1089778

De Baar, H. J. W., J. T. M. de Jong, D. C. E. Bakker, B. M. Löscher, C. Veth, U. Bathmann, and V. Smetacek. 1995.

Importance of iron for plankton blooms and carbon dioxide drawdown in the Southern Ocean. Nature **373**: 412–415. doi:10.1038/373412a0

El-Sayed, S. Z. 2005. History and evolution of primary productivity studies of the Southern Ocean. Polar Biol. **28**: 423–438. doi:10.1007/s00300-004-0685-2

Enderlein, J., and R. Erdmann. 1997. Fast fitting of multi-exponential decay curves. Opt. Commun. **134**: 371–378. doi:10.1016/S0030-4018(96)00384-7

Falkowski, P. G., M. Greene, and R. J. Geider. 1992. Physiological limitations on phytoplankton productivity in the ocean. Oceanography **5**: 84–91. doi:10.5670/oceanog.1992.14

Falkowski, P. G., M. E. Katz, A. H. Knoll, A. Quigg, J. A. Raven, O. Schofield, and F. J. R. Taylor. 2004. The evolution of modern eukaryotic phytoplankton. Science **305**: 354–360. doi:10.1126/science.1095964

Gerringa, L. J. A., and others. 2012. Iron from melting glaciers fuels the phytoplankton blooms in Amundsen Sea (Southern Ocean): Iron biogeochemistry. Deep-Sea Res. Part II **71–76**: 16–31. doi:10.1016/j.dsr2.2012.03.007

Gervais, F., U. Riebesell, and M. Y. Gorbunov. 2002. Changes in primary productivity and chlorophyll a in response to Iron fertilization in the Southern Polar Frontal Zone. Limnol. Oceanogr. **47**: 1324–1335. doi:10.4319/lo.2002.47.5.1324

Gorbunov, M. Y., S. Kolber, and P. G. Falkowski. 1999. Measuring photosynthetic parameters in individual algal cells by Fast Repetition Rate fluorometry. Photosynth. Res. **62**: 141–153. doi:10.1023/A:1006360005033

Gorbunov, M. Y., G. Falkowski, and Z. S. Kolber. 2000. Measurement of photosynthetic parameters in benthic organisms in situ using a SCUBA-based fast repetition rate fluorometer. Limnol. Oceanogr. **45**: 242–245. doi:10.4319/lo.2000.45.1.0242

Gorbunov, M. Y., S. Kolber, M. P. Lesser, and P. G. Falkowski. 2001. Photosynthesis and photoprotection in symbiotic corals. Limnol. Oceanogr. **46**: 75–85. doi:10.4319/lo.2001.46.1.0075

Gorbunov, M. Y., and P. G. Falkowski. 2005. Fluorescence induction and relaxation (FIRe) technique and instrumentation for monitoring photosynthetic processes and primary production in aquatic ecosystems, p. 1029–1031. *In* A. Van der Est and D. Bruce [eds.], Photosynthesis fundamental. Intenational Society of Photosynthesis Aspects to Global Perspectives.

Greene, R. M., J. Geider, and P. G. Falkowski. 1991. Effect of iron limitation on photosynthesis in a marine diatom. Limnol. Oceanogr. **36**: 1772–1782. doi:10.4319/lo.1991.36.8.1772

Greene, R. M., J. Geider, Z. Kolber, and P. G. Falkowski. 1992. Iron-induced changes in light harvesting and photochemical energy conversion processes in eukaryotic marine algae. Plant Physiol. **100**: 565–575. doi:10.1104/pp.100.2.565

Holm-Hansen, O., and B. G. Mitchell. 1991. Spatial and temporal distribution of phytoplankton and primary production in the western Bransfield Strait region. Deep-Sea Res. **38**: 961–980. doi:10.1016/0198-0149(91)90092-T

Hopkinson, B. M., and others. 2007. Iron limitation across chlorophyll gradients in the southern Drake Passage: Phytoplankton responses to iron addition and photosynthetic indicators of iron stress. Limnol. Oceanogr. **52**: 2540–2554. doi:10.4319/lo.2007.52.6.2540

Jacobs, S. S., A. Jenkins, C. F. Giulivi, and P. Dutrieux. 2011. Stronger ocean circulation and increased melting under Pine Island Glacier ice shelf. Nat. Geosci. **4**: 519–523. doi:10.1038/ngeo1188

Jassby, A. D., and T. Platt. 1976. Mathematical formulation of the relationship between photosynthesis and light for phytoplankton. Limnol. Oceanogr. **21**: 540–547. doi:10.4319/lo.1976.21.4.0540

Jenkins, A., P. Dutrieux, S. S. Jacobs, S. D. McPhail, J. R. Perrett, A. T. Webb, and D. White. 2010. Observations beneath Pine Island Glacier in West Antarctica and implications for its retreat. Nat. Geosci. **3**: 468–472. doi:10.1038/ngeo890

Kolber, Z. S., O. Prasil, and P. G. Falkowski. 1998. Measurements of variable chlorophyll fluorescence using fast repetition rate techniques: Defining methodology and experimental protocols. BBA Bioenergetics **1367**: 88–106. doi:10.1016/S0005-2728(98)00135-2

Korb, R. E., J. Whitehouse, and P. Ward. 2004. SeaWiFS in the southern ocean: Spatial and temporal variability in phytoplankton biomass around South Georgia. Deep-Sea Res. Part II **51**: 99–116. doi:10.1016/j.dsr2.2003.04.002

Krause, G. H., and E. Weis. 1991. Chlorophyll fluorescence and photosynthesis: The basics. Annu. Rev. Plant Physiol. Plant Mol. Biol. **42**: 313–349. doi:10.1146/annurev.pp.42.060191.001525

Kuzminov, F. I., and M. Y. Gorbunov. 2016. Energy dissipation pathways in Photosystem 2 of the diatom, Phaeodactylum tricornutum, under high-light conditions. Photosynth. Res. **127**: 219–235. doi:10.1007/s11120-015-0180-3

Lakowicz, J. R. 2006. Principles of fluorescence spectroscopy, 3rd ed. Springer Science+Business Media, LLC.

Landry, M. R., and R. P. Hassett. 1982. Estimating the grazing impact of marine micro-zooplankton. Mar. Biol. **67**: 283–288. doi:10.1007/BF00397668

Lee, S., B. K. Kim, M. S. Yun, H. Joo, E. J. Yang, Y. N. Kim, H. C. Shin, and S. Lee. 2012. Spatial distribution of phytoplankton productivity in the Amundsen Sea, Antarctica. Polar Biol. **35**: 1–13. doi:10.1007/s00300-012-1220-5

Lin, H., F. I. Kuzminov, J. Park, S. Lee, P. G. Falkowski, and M. Y. Gorbunov. 2016. The fate of photons absorbed by

phytoplankton in the global ocean. Science **351**: 264–267. doi:10.1126/science.aab2213

Martin, J. H., M. Gordon, and S. E. Fitzwater. 1990. Iron in Antarctic waters. Nature **345**: 156–158. doi:10.1038/345156a0

Mitchell, B. G., and O. Holm-Hansen. 1991. Observations of modeling of the Antartic phytoplankton crop in relation to mixing depth. Deep-Sea Res. **38**: 981–1007. doi:10.1016/0198-0149(91)90093-U

Mu, L., S. E. Stammerjohn, K. E. Lowry, and P. L. Yager. 2014. Spatial variability of surface pCO2 and air-sea CO2 flux in the Amundsen Sea Polynya, Antarctica. Elementa **2**: 000036. doi:10.12952/journal.elementa.000036

Nelson, D. M., and W. O. Smith. 1991. Sverdrup revisited - critical depths, maximum chlorophyll levels, and the control of Southern-Ocean productivity by the irradiance-mixing regime. Limnol. Oceanogr. **36**: 1650–1661. doi:10.4319/lo.1991.36.8.1650

Olson, R. J., M. Sosik, A. M. Chekalyuk, and A. Shalapyonok. 2000. Effects of iron enrichment on phytoplankton in the Southern Ocean during late summer: Active fluorescence and flow cytometric analyses. Deep-Sea Res. II **47**: 3181–3200. doi:10.1016/S0967-0645(00)00064-3

Park, J., I.-S. Oh, H.-C. Kim, and S. Yoo. 2010. Variability of SeaWiFs chlorophyll-a in the southwest Atlantic sector of the Southern Ocean: Strong topographic effects and weak seasonality. Deep-Sea Res. **57**: 604–620. doi:10.1016/j.dsr.2010.01.004

Park, J., and others. 2013. Early summer iron limitation of phytoplankton photosynthesis in the Scotia Sea as inferred from fast repetition rate fluorometry. J. Geophys. Res. **118**: 3795–3806. doi:10.1002/jgrc.20281

Parsons, T. R., Y. Maita, and C. M. Lalli. 1984. A manual of chemical and biological methods for seawater analysis. Pergamon Press.

Peloquin, J. A., and W. O. Smith, Jr. 2007. Phytoplankton blooms in the Ross Sea, Antarctica: Interannual variability in magnitude, temporal patterns, and composition. J. Geophys. Res. **112**: C08013. doi:10.1029/2006JC003816

Rignot, E., J. L. Bamber, M. R. van den Broeke, C. Davis, Y. Li, W. J. van de Berg, and E. van Meijgaard. 2008. Recent Antarctic ice mass loss from radar interferometry and regional climate modelling. Nat. Geosci. **1**: 106–110. doi:10.1038/ngeo102

Schofield, O., and others. 2015. In situ phytoplankton distributions in the Amundsen Sea Polynya measured by autonomous gliders. Elementa **3**: 000073. doi:10.12952/journal.elementa.000073

Schrader, P. S., J. Milligan, and M. J. Behrenfeld. 2011. Surplus photosynthetic antennae complexes underlie diagnostics of iron limitation in a cyanobacterium. Plos One **6**: e18753. doi:10.1371/journal.pone.0018753 doi:10.1371/journal.pone.0018753

Sedwick, P. N., R. Ditullio, and D. J. Mackey. 2000. Iron and manganese in the Ross Sea, Antarctica: Seasonal iron limitation in Antarctic shelf waters. J. Geophys. Res. **105**: 11321–11336. doi: 10.1029/2000JC000256

Sherrell, R. M., M. Lagerstrom, K. O. Forsch, S. E. Stammerjohn, and P. L. Yager. 2015. Dynamics of dissolved iron and other bioactive trace metals (Mn, Ni, Cu, Zn) in the Amundsen Sea Polynya, Antarctica. Elementa **3**: 000071. doi:10.12952/journal.elementa.000071

Smetacek, V., and U. Passow. 1990. Spring bloom initiation and Sverdrup's critical-depth model. Limnol. Oceanogr. **35**: 228–234. doi:10.4319/lo.1990.35.1.0228

Smith, K. L., B. H. Robison, J. J. Helly, R. S. Kaufmann, H. A. Ruhl, T. J. Shaw, B. S. Twining, and M. Vernet. 2007. Free-drifting Icebergs: Hot spots of chemical and biological enrichment in the Weddell Sea. Science **317**: 478–482. doi:10.1126/science.1142834

Smith, W. O., Jr., and J. C. Comiso. 2008. Influence of sea ice on primary production in the Southern Ocean: A satellite perspective. J. Geophys. Res. **113**: C05S93. doi:10.1029/2007JC004251

Smith, W. O., Jr., and others. 2013. Spatial and temporal variations in variable fluoresence in the Ross Sea (Antarctica): Oceanographic correlates and bloom dynamics. Deep-Sea Res. Part I **79**: 141–155. doi:10.1016/j.dsr.2013.05.002

Suggett, D. J., M. Moore, A. E. Hickman, and R. J. Geider. 2009. Interpretation of fast repetition rate (FRR) fluorescence: Signatures of phytoplankton community structure versus physiological state. Mar. Ecol. Prog. Ser. **376**: 1–19. doi:10.3354/meps07830

Sunda, W. G., and S. A. Huntsman. 1997. Interrelated influence of iron, light and cell size on marine phytoplankton growth. Nature **390**: 389–392. doi:10.1038/37093

Sverdrup, H. U. 1953. On conditions for the vernal blooming of phytoplankton. J. Cons. **18**: 287–295. doi:10.1093/icesjms/18.3.287

Tagliabue, A., and K. R. Arrigo. 2005. Iron in the Ross Sea: 1. Impact on CO2 fluxes via variation in phytoplankton functional group and non-Redfield stoichiometry. J. Geophys. Res. **110**: C03009. doi:10.1029/2004JC002531

Thuróczy, C.-E., A.-C. Alderkamp, P. Laan, L. J. A. Gerringa, M. M. Mills, G. L. Van Dijken, H. J. W. De Baar, and K. R. Arrigo. 2012. Key role of organic complexation of iron in sustaining phytoplankton blooms in the Pine Island and Amundsen Polynyas (Southern Ocean). Deep-Sea Res. Part II **71–76**: 49–60. doi:10.1016/j.dsr2.2012.03.009

Vassiliev, I. R., Z. Kolber, K. D. Wyman, D. Mauzerall, V. K. Shukla, and P. G. Falkowski. 1995. Effects of iron limitation on photosystem II composition and light utilization in Dunaliella tertiolecta. Plant Physiol. **109**: 963–972. doi:10.1104/pp.109.3.963

Vaughan, D. 2008. West Antarctic Ice Sheet collapse – the fall and rise of a paradigm. Clim. Change **91**: 65–79. doi: 10.1007/s10584-008-9448-3

Wåhlin, A. K., X. Yuan, G. Björk, and C. Nohr. 2010. Inflow of warm circumpolar deep water in the central Amundsen shelf. J. Phys. Oceanogr. **40**: 1427–1434. doi:10.1175/2010JPO4431.1

Walker, D. P., A. Brandon, A. Jenkins, J. T. Allen, J. A. Dowdeswell, and J. Evans. 2007. Oceanic heat transport onto the Amundsen Sea shelf through a submarine glacial trough. Geophys. Res. Lett. **34**: L02602. doi:10.1029/2006GL028154

Yang, E. J., Y. Jiang, and S. Lee. 2016. Microzooplankton herbivory and community structure in the Amundsen Sea, Antarctica. Deep-Sea Res. Part II **123**: 58–68. doi:10.1016/j.dsr2.2015.06.001

Acknowledgments

We thank members of the A-team, the captain and the crew of the R/V *Araon*. We thank anonymous reviewers and the editor for constructive comments on the manuscript, David Suggett, Hugh Ducklow, Oscar Schofield and Kevin Wyman for comments. This research was supported by Grant PE17060 from the Korea Polar Research Institute (to JP and SL) and Grant NNX16AT54G from NASA Ocean Biology and Biogeochemistry Program (to MYG and PGF).

Conflict of Interest

None declared.

Submitted 17 June 2016
Revised 11 January 2017; 03 March 2007
Accepted 09 March 2017

Associate editor: James Moffett